# ENERGETIC PARTICLES IN THE SOLAR ATMOSPHERE

N. Vilmer[1] and S. Musset[2]

**Abstract.** The Sun is an efficient particle accelerator. These particles play a major role in the active Sun because they contain a large amount of the magnetic energy released during flares. Energetic electrons and ions interact with the solar atmosphere and produce high-energy X-rays and $\gamma$-rays. Energetic particles can also escape to the corona and interplanetary medium and may eventually reach the Earth's orbit. It is currently admitted that solar flares are powered by magnetic energy previously stored in the coronal magnetic field and that magnetic energy release is likely to occur on coronal current sheets along regions of strong gradient of magnetic connectivity. Particle transport from the acceleration region to the emission sites must also be considered to infer properties of the accelerated particles (and thus of the acceleration processes) from the observations of their radiation. In this paper, we will present the results of some recent studies using RHESSI observations: relationship found in some flares between ribbons of electric currents observed at the photospheric level and the flare energetic electrons traced by their X-ray emissions. We will also present some results on electron transport in solar flares and comment on the role of scattering in this process. We will finally describe some recent results from FERMI/LAT observations on the production of GeV protons in connection with solar flares and/or coronal mass ejections.

Keywords: Sun, Solar Flares, Energetic Particles, X-ray, $\gamma$- ray, RHESSI, FERMI/LAT

## 1 Introduction

The Sun is a powerful particle accelerator.This has been known since the first detection of solar energetic protons by ground-based neutron monitors in 1942, the first detection of solar flares in radio and X-rays, in the 1970s and the first observations of $\gamma$-ray lines in 1972. Since then, many observations of solar X-ray flares have been observed with several solar-dedicated missions. The last of this mission is the RHESSI (Reuven Ramaty High Energy Solar Spectroscopic) mission (Lin et al. 2002) which observed more than 120000 X-ray flares above 6 keV between 2002 and 2018. If this large amount of HXR observations has provided a substantial knowledge of electron acceleration in solar flares, our knowledge on ion acceleration in flares is still limited given the total number of $\gamma$-ray line flares ($< 30$) which has been observed both by solar-dedicated and general $\gamma$-ray missions. Recent FERMI/LAT $\gamma$-ray observations have however shown that the production of relativistic ($>$ GeV) protons in flares and eruptions is more common than previously expected and may last for several hours after the main flaring episode at the Sun. The most direct quantitative diagnostics of energetic particles interacting at the Sun come from HXR/ $\gamma$-ray observations. They carry information on electron and ion energy spectra, numbers, energy contents and abundances of accelerated ions. While bremsstrahlung X-ray continuum emission observed from 1 keV to 100 MeV provides diagnostic information about energetic electrons, $\gamma$-ray lines from 0.5 to 8 MeV tell us about ions above a few MeV/nuc in energy, and the continuum above 100 MeV (pion decay radiation) yields information about ions $> 0.2$ GeV/nuc (e.g. Share & Murphy 2006, Vilmer et al. 2011, Vilmer 2012 for reviews). This paper is focussed on the X-ray part of the RHESSI observations(dealing mostly with energetic electrons) and on the input ot the recent FERMI/LAT observations (dealing with the highest energetic protons).

## 2 Energetic electron acceleration and transport in solar flares

Figure 1 shows a typical X-ray flare spectrum observed with RHESSI between 3 and 100 keV. At energies up to 10-20 keV (depending on the event) the emision is dominated by emission from the hot plasma ($\simeq 30$

---

[1] LESIA, Observatoire de Paris, Université PSL, CNRS, Sorbonne Université, Université de Paris, 5 place Jules Janssen, 92195 Meudon, France

[2] School of Physics and Astronomy, University of Minnesota, 116 Church St SE, Minneapolis, MN 55455, USA
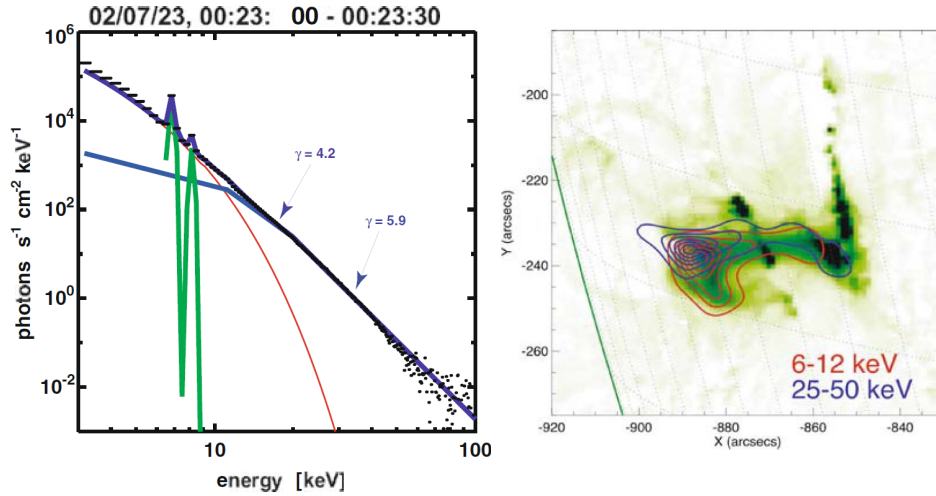
**Fig. 1. Left:** photon spectrum showing thermal emission (red) including the Fe and Fe/Ni line complexes in green (Phillips 2004), and the non-thermal emission in blue. **Right:** RHESSI contours in the thermal range (red) and at higher energies in the non-thermal range. The image shown is a TRACE 195 Å image taken at 00:26:00 UTC (from Krucker et al. 2008)

MK) (thermal free-free and free-bound continua as well as two line features at $\simeq 6.7$ and 8 keV coming from Fe and Fe/Ni line complexes). Bremsstrahlung emission from non-thermal electrons (typically above $\simeq 10$ keV) produces the non-thermal part of the HXR spectrum. RHESSI images usually show that the thermal emission comes from magnetic loops filled with hot plasma above the flare brightening (ribbons) seen here in EUV. The emission from non-thermal electrons usually comes from footpoints (which reveal the interaction sites of the energetic electrons with the dense chromosphere). In addition with the HXR footpoint sources, strong HXR sources are sometimes observed in the corona (Figure 2). This indicates the presence of high energy particles confined in the corona which can either trace the acceleration or trapping sites. In the context of solar flares, the source of the energy going to energetic particles is the magnetic energy stored in non-potential magnetic fields which can be released due to magnetic reconnection. From observations and models of the emissions, the general questions are related to the link between plasma heating and particle acceleration, the nature of the acceleration mechanisms and the conditions under which acceleration mechanisms operate, the location of the acceleration sites and the transport of particles from acceleration sites to X-ray emitting sites mostly present in dense regions of the solar atmosphere. As in all astrophysical plasmas, several acceleration mechanisms are possible: acceleration by shocks linked to the reconnection processes, stochastic acceleration by e.g. wave-particle interaction or direct electric field acceleration in connection e.g. reconnecting current sheets.

### 2.1 High energy electrons and Electric Currents in Solar Flares

It is commonly accepted that solar flares are the result of the sudden release of magnetic energy stored in non-potential magnetic fields associated with electric currents in the corona. Electric currents can be derived from vector magnetic field measurements which are mostly achieved at the photospheric level. Therefore, only measurements of photospheric electric currents can be deduced from the observations. Polarimetric measurements obtained continuously with high temporal and spatial resolution with the Helioseismic and Magnetic Imager (HMI) aboard Solar Dynamic Observatory (SDO) allow to derive maps of photospheric vertical electric currents for flaring active regions at a time cadence of 12min (or less) which allows to study the evolution of currents on a flare timescale (Petrie 2012; Janvier et al. 2014; Musset et al. 2015; Sharykin et al. 2019). The combination of these polarimetric measurements with RHESSI HXR images allows the comparison of electric current maps and electron interaction/acceleration sites during flares.

Figure 3 shows the first published comparison of the evolution with time of hard X-ray sources and of the current density maps at the photospheric level. The observations reveal a good spatial correlation between
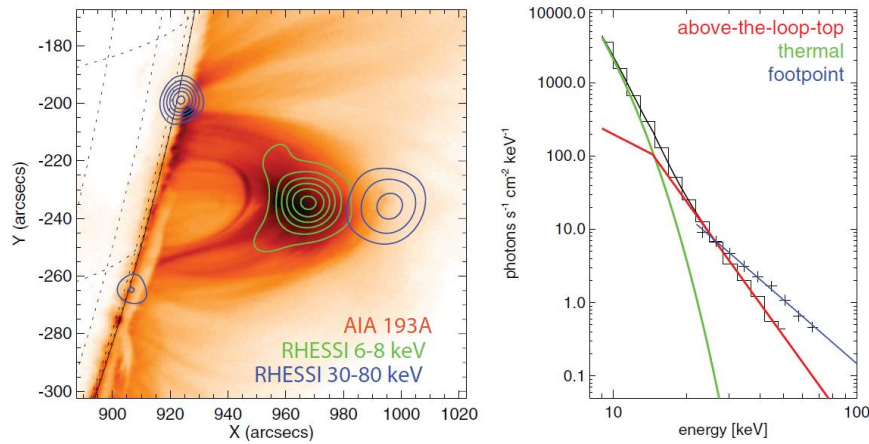
**Fig. 2. Left:** The thermal emissions (green contours) in the 6-8 keV range show the location of the main flare loops also seen in the 193 Å AIA image. The non-thermal HXR emissions come from the footpoints of the thermal flare loops, but also from above the main flare loop as outlined by the 30-80 keV (blue) contours. **Right:** imaging spectroscopy results: the black histogram gives the imaging spectroscopy results for the combined coronal sources; the observed footpoint spectrum is given by crosses. The green and red curves are the thermal and non-thermal fit to the combined coronal sources, while the power-law fit to the footpoints is given in blue. (Krucker & Battaglia 2014)
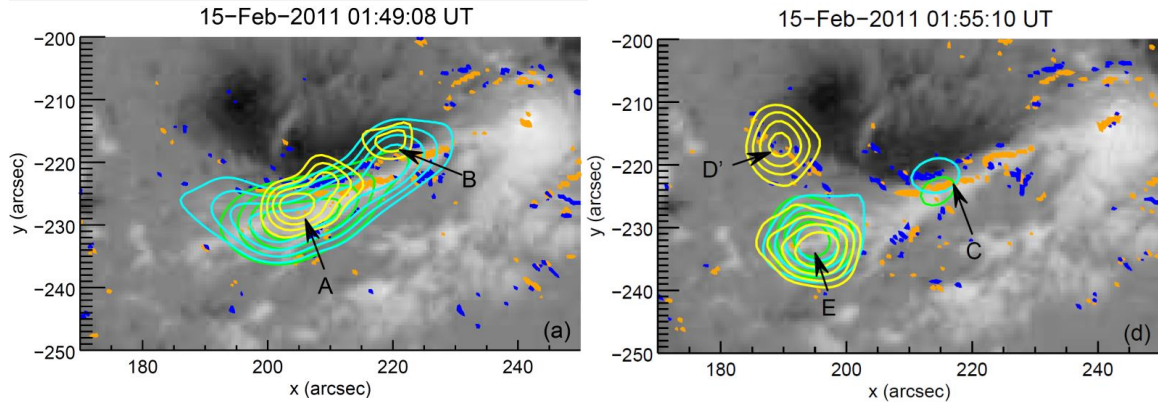


**Fig. 3. Left:** Magnetic field map (in grey scale) from SDO/HMI on February 15, 2011, at 01:48:00 UT (left) overlaid with positive and negative vertical electric current densities, respectively, with amplitude>100 mA/m$^2$ and RHESSI contours at 12 - 25 keV, 25 - 50 keV, and 50 - 100 keV (green, cyan, yellow) integrated between 01:49:00 and 01:49:16 UT **Right:** Same for magnetic field map and electric currents at 02:00:00 UT and RHESSI contours integrated between 01:55:02 and 01:55:18 (from Musset et al. 2015)

photospheric current ribbons (interpreted as footprints of coronal electric currents (Janvier et al. 2014) and the coronal elongated X-ray sources observed between 12 and 50 keV (figure 3 left) indicative of the acceleration region. A coincident appearance of a new X-ray source at 50-100 keV (D') and of new vertical electric currents in the same region (Musset et al. 2015) is also observed (figure 3 right). These observational results can be interpreted in the context of magnetic reconnection and subsequent electron acceleration preferentially occurring at current-carrying (reconnecting) sheets in the corona.
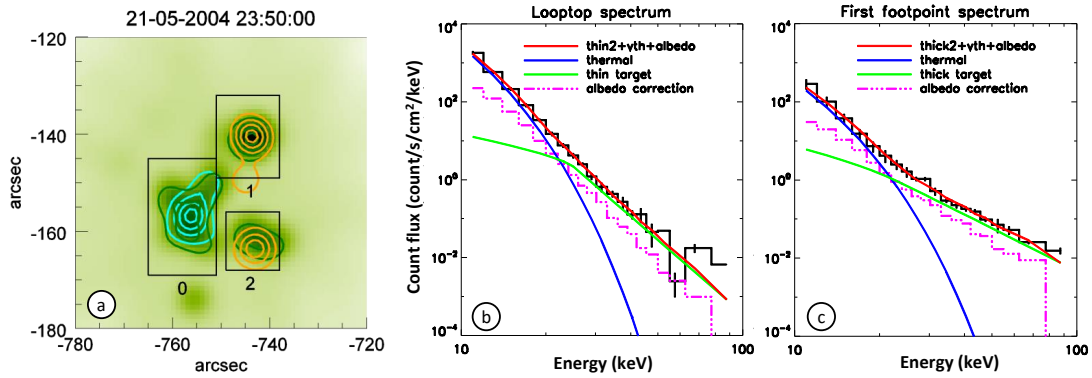
**Fig. 4.** (a) X-ray image between 23:49:30 and 23:50:30 UT at 25-50 keV overlaid with contours at 10-25 keV (blue), 25-50 keV (green), and 50-100 keV (orange). Boxes 0, 1, 2 are used for imaging spectroscopy of the looptop source, the first footpoint, and the second footpoint, respectively. Count flux spectra (data and fit) with residuals for looptop source (b), first footpoint (c), as defined by the black boxes in (a). The spectra derived from the data are shown in black. The blue curve represents the thermal component of the fit and the green curve represents the non-thermal component. The red curve indicates the total fitted spectrum.The thermal emissions in the 6-8 keV range show the location of the main flare loops also seen in the 193 Å AIA image. (Musset et al. 2018)

## 2.2   Transport of energetic electrons in the solar corona

As mentioned above, energetic electrons are believed to be accelerated in the low corona and to produce X-ray emissions dominantly in the chromosphere. Therefore, particle transport must be studied and evaluated since it can modify the spatial and spectral characteristics of the energetic particles produced in the acceleration region. Imaging spectroscopy capabilities provided by RHESSI has allowed to study transport effects in an unprecedented manner by measuring X-ray producing electron spectra in the coronal source (close to the presumed acceleration region) and in the footpoints (e.g. Battaglia & Benz 2006, Simões & Kontar 2013, Musset et al. 2018). Figure 4 shows one the event for which imaging spectroscopy has been performed. The results of the analysis show that the energetic electron spectra derived from the X-ray analysis in the corona and in the footpoints are different and that the non-thermal electron rate in the coronal source is larger by a ratio of 2.2 than the footpoint rate. This shows that in these events the transport of electrons from the acceleration site to the dense emitting footpoint does not agree with the standard transport model (e.g. Syrovatskii & Shmeleva 1972) in which energetic electrons accelerated in the corona propagate freely along the magnetic field lines of coronal loops losing only a small amount of energy through collisions with the ambient plasma until they real the dense footpoints. Both the hardening of the electron spectrum during the transport from the corona to the footpoints and the larger electron rate in the coronal source can be explained by trapping of electrons in the coronal part of the loop (Musset et al. 2018). Such a confinement at the top of a loop can be due to magnetic mirroring (e.g. Kennel & Petschek 1966; Melrose & Brown 1976; Vilmer et al. 1986) or to confinement by strong turbulent pitch-angle scattering due to small scale magnetic field fluctuations leading to diffusive parallel transport (e.g. Bian et al. 2011; Kontar et al. 2014). In the last case, the comparison of observations with the results of a diffusive transport model allows to deduce the scattering mean free path of electrons. For the event shown in Figure 4, the mean free path for electron energies between 25 and 100 keV is around $1.4 \times 10^8$ cm. Radio observations of the same event achieved with the Nobeyama Radioheliograph also show evidence of the confinement of radio emitting electrons (energies around 400 keV) in the corona. The confinement is however stronger for these higher energy electrons ($10^7$ cm) showing a decrease with energy of the scattering mean free path of energetic electrons in the corona. This is the first report of such an effect in the low corona. Similar dependence of the scattering mean free path over electron energies has been also found in the case of interplanetary electron transport (e.g. Agueda et al. 2014) and must related to the properties of the scattering agents.
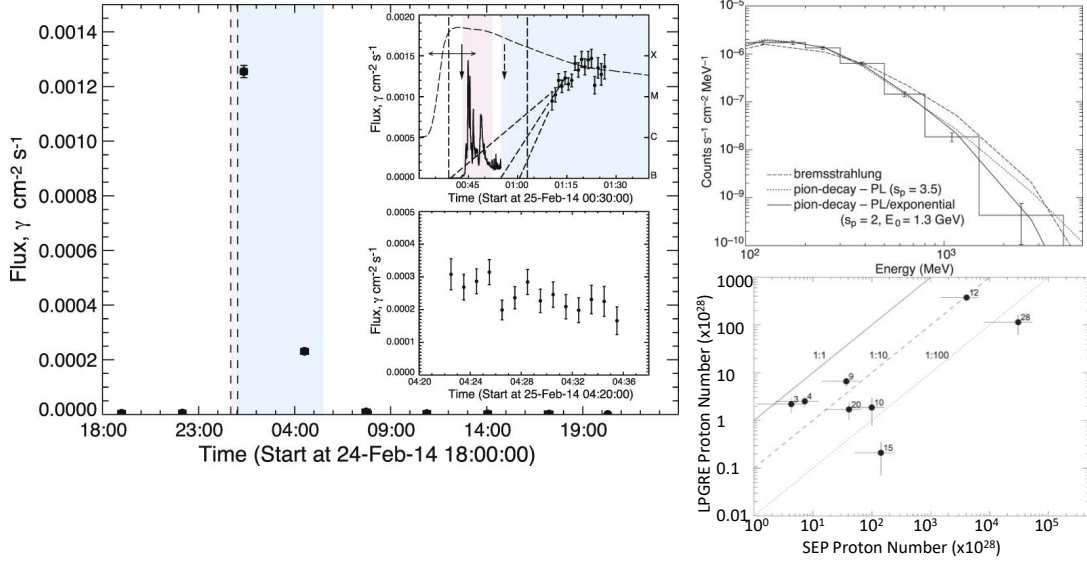
**Fig. 5. Left:** Time profile of the 2014 February 25 long duration event observed by FERMI/LAT above 100 MeV. *The top inset* shows RHESSI 100-300 keV rates (thick line in pink shaded region) plotted on the same scale as > 100 MeV $\gamma$-ray fluxes (points). The pink and blue shaded regions indicate the time intervals for the impulsive $\gamma$-ray emission and the late phase $\gamma$-ray emission respectively. The dashed curve shows the GOES time history. *The bottom inset* is a blowup of the time profile after 04:24 UT second showing a declining $\gamma$-ray flux. **Top right:** Background-subtracted LAT count spectrum with $\pm 1\,\sigma$ statistical uncertainties measured with LAT between 01:13:30 and 01:17:30 UT. Best fits to the observed count spectrum are shown: (1) a pion-decay spectrum produced by a power-law spectrum of protons with spectral index $s_p = 3.5$ (dotted curve); (2) a pion-decay spectrum produced by a power-law spectrum of protons with spectral index $s_p = 2$ and 1.3 GeV exponential cutoff energy (solid curve); and (3) a bremsstrahlung spectrum produced at a density of $10^{16}$ cm$^{-3}$ from a power-law spectrum of primary electrons with index $s = 1$ and 1 GeV exponential cutoff energy, in a $10^3$ G magnetic field (dashed curve). **Bottom right:** Number of > 500 MeV protons producing the late > 100 MeV $\gamma$-ray event vs. the estimated number in the associated SEP event. The lines represent ratios of 1:1, 1:10, and 1:100 (from Share et al. 2018)

## 3 FERMI/LAT observations of long duration $\gamma$-ray events

Previous to the arrival of new data from FERMI/LAT, around 20 solar events had been observed with significant emission above 60 MeV from pion decay radiation (see Chupp & Ryan 2009; Vilmer et al. 2011 for reviews and Forrest et al. 1985 and Murphy et al. 1987 for the first observations and interpretations with Solar Maximum Mission). For some of the events, pion decay radiation is observed during the impulsive phase of the event as defined by the production of hard X-rays above 100 keV, but some events show extended pion decay radiation lasting for several hours (Kanbach et al. 1993; Ryan 2000;Rank et al. 2001). Several interpretations were proposed to explain these long duration emissions, either continuous acceleration of protons above 300 MeV (see e.g. Ryan & Lee 1991) or trapping of protons on very long time-scales. In particular, Mandzhavidze & Ramaty 1992 showed that the long duration phase could be explained by the injection of energetic protons in the impulsive phase and subsequent trapping. An efficient trapping on such long timescales required a strong mirror ratio in the trapping region (>10) as well as a coronal density less than $5 \times 10^{11}$ cm$^{-3}$.

FERMI/LAT more sensitive observations provided new surprising results. High energy emission above 100 MeV was first detected for a "weak" impulsive GOES M2 class flare (Ackermann et al. 2012) and around $\simeq$ 30 solar events were reported above 100 MeV (Ackermann et al. 2014). FERMI/LAT observations also allows to deduce the location of the centroid of the $\gamma$-ray source above 1 GeV and to show that these locations are consistent with the location of solar flaring active regions even in the case of sustained emissions (see e.g. Klein et al. 2018 for a review).

In a recent study, Share et al. (2018) analyzed 30 events with late phase > 100 MeV $\gamma$-ray emissions (see figure 5 left). For most of the events (27 events) the spectral analysis shows that spectra are consistent with pion decay radiation produced by > 300 MeV protons and are not consistent with relativistic electron bremsstrahlung

emissions (see e.g. figure 5 top right). This confirms that the Sun is able to produce a significant number of high energy protons ($> 300$ MeV) for several hours after the impulsive flare. The number of accelerated protons above 500 MeV interacting at the Sun can be then deduced from the derived pion decay spectrum using the models developed in Murphy et al. (1987). The number of protons above 500 MeV is in the range $10^{27}$ - $10^{30}$ and is at least a factor of 10 larger than the number of protons above 500 MeV which is responsible for the production of the impulsive $> 100$ Mev $\gamma$-ray emission when observed (see Share et al. 2018). Figure 5 bottom right panel shows the comparison for 8 events of the number of $> 500$ Mev protons producing the late $> \gamma$-ray emissions and of the number of $> 500$ MeV protons emitted at the vicinity of the Sun and propagating in the interplanetary medium (see Share et al. 2018). It is found that the number of $> 500$ Mev protons needed to produce the late high energy $\gamma$- rays is 0.1 to 50 % of the number of protons of the associated interplanetary event.

The recent FERMI/LAT results initiated new discussions on the origin of the long duration high energy radiation which is most of the time not accompanied by any other radiative signature apart from a type II radio emission indicative of the production of a shock wave propagating from the corona to the interplanetary medium and usually associated with a coronal mass ejection (see e.g. Klein et al. 2018). Several papers have recently addressed the origin of this long lasting radiation, attributing their production to energetic protons escaping the turbulent downstream region of the CME shock back to the Sun along converging field lines (e.g. Jin et al. 2018) or accelerated by the CME shock and going back to the solar surface (e.g. Plotnikov et al. 2017).

## 4   Conclusions

High energy emission during solar flares is a powerful diagnostics of the fundamental processes of magnetic energy release, particle acceleration and transport in the solar corona. X-ray and $\gamma$-ray observations provide information on solar energetic particles at their source. RHESSI and Fermi/LAT provide novel observations of energetic particle during solar flares, but also raise new questions and challenge our understanding of particle acceleration and transport during these events. Among the next observational challenges lie the observation of faint X-ray emission in the corona, supposedly close or in the acceleration region, and imaging of the pion-decay radiation during solar flares. The next solar-dedicated X-ray spectro-imager, STIX, on Solar Orbiter, will provide observations at high sensitivity and high temporal cadence. Focusing optics for solar X-ray observation, as demonstrated by the FOXSI sounding rocket, is under consideration to provide X-ray imaging spectroscopy with a high sensitivity and high dynamic range. A white paper on Solar Particle Acceleration, Radiation and Kinetics (SPARK) has been proposed by Matthews and collaborators to the ESA Voyager 2050 call promoting a future solar $\gamma$-ray mission. The combination of these diagnostics of the sources of energetic particles that can escape and propagate through the heliosphere with the in-situ measurements of particles close to the Sun in the heliosphere that are possible with Solar Orbiter and Parker Solar Probe, will greatly improve our understanding of particle acceleration and transport in our heliosphere.

## References

Ackermann, M., Ajello, M., Albert, A., et al. 2014, ApJ, 787, 15

Ackermann, M., Ajello, M., Allafort, A., et al. 2012, ApJ, 745, 144

Agueda, N., Klein, K. L., Vilmer, N., et al. 2014, A&A, 570, A5

Battaglia, M. & Benz, A. O. 2006, A&A, 456, 751

Bian, N. H., Kontar, E. P., & MacKinnon, A. L. 2011, A&A, 535, A18

Chupp, E. L. & Ryan, J. M. 2009, Research in Astronomy and Astrophysics, 9, 11

Forrest, D. J., Vestrand, W. T., Chupp, E. L., et al. 1985, in International Cosmic Ray Conference, Vol. 4, 19th International Cosmic Ray Conference (ICRC19), Volume 4, 146

Janvier, M., Aulanier, G., Bommier, V., et al. 2014, ApJ, 788, 60

Jin, M., Petrosian, V., Liu, W., et al. 2018, ApJ, 867, 122

Kanbach, G., Bertsch, D. L., Fichtel, C. E., et al. 1993, A&AS, 97, 349

Kennel, C. F. & Petschek, H. E. 1966, J. Geophys. Res., 71, 1

Klein, K.-L., Tziotziou, K., Zucca, P., et al. 2018, in Solar Particle Radiation Storms Forecasting and Analysis, ed. O. E. Malandraki & N. B. Crosby, Vol. 444, 133–155

Kontar, E. P., Bian, N. H., Emslie, A. G., & Vilmer, N. 2014, ApJ, 780, 176

Krucker, S. & Battaglia, M. 2014, ApJ, 780, 107

Krucker, S., Battaglia, M., Cargill, P. J., et al. 2008, A&A Rev., 16, 155

Lin, R. P., Dennis, B. R., Hurford, G. J., et al. 2002, Sol. Phys., 210, 3

Mandzhavidze, N. & Ramaty, R. 1992, ApJ, 396, L111

Melrose, D. B. & Brown, J. C. 1976, MNRAS, 176, 15

Murphy, R. J., Dermer, C. D., & Ramaty, R. 1987, ApJS, 63, 721

Musset, S., Kontar, E. P., & Vilmer, N. 2018, A&A, 610, A6

Musset, S., Vilmer, N., & Bommier, V. 2015, A&A, 580, A106

Petrie, G. J. D. 2012, Sol. Phys., 281, 577

Phillips, K. J. H. 2004, ApJ, 605, 921

Plotnikov, I., Rouillard, A. P., & Share, G. H. 2017, A&A, 608, A43

Rank, G., Ryan, J., Debrunner, H., McConnell, M., & Schönfelder, V. 2001, A&A, 378, 1046

Ryan, J. M. 2000, Space Sci. Rev., 93, 581

Ryan, J. M. & Lee, M. A. 1991, ApJ, 368, 316

Share, G. H. & Murphy, R. J. 2006, Washington DC American Geophysical Union Geophysical Monograph Series, 165, 177

Share, G. H., Murphy, R. J., White, S. M., et al. 2018, ApJ, 869, 182

Sharykin, I. N., Zimovets, I. V., & Myshyakov, I. I. 2019, arXiv e-prints, arXiv:1905.03352

Simões, P. J. A. & Kontar, E. P. 2013, A&A, 551, A135

Syrovatskii, S. I. & Shmeleva, O. P. 1972, Soviet Ast., 16, 273

Vilmer, N. 2012, Philosophical Transactions of the Royal Society of London Series A, 370, 3241

Vilmer, N., MacKinnon, A. L., & Hurford, G. J. 2011, Space Sci. Rev., 159, 167

Vilmer, N., Trottet, G., & MacKinnon, A. L. 1986, A&A, 156, 64